NON-INTRUSIVE TEMPERATURE DIAGNOSTIC FOR A NON-NEUTRAL PLASMA

by

Michael Takeshi Nakata

A thesis submitted to the faculty of

Brigham Young University

in partial fulfillment of the requirements for the degree of

Master of Science

Department of Physics and Astronomy

Brigham Young University

April 2002

BRIGHAM YOUNG UNIVERSITY

GRADUATE COMMITTEE APPROVAL

of a thesis submitted by

Michael Takeshi Nakata

This thesis has been read by each member of the following graduate committee and by majority vote has been found to be satisfactory.

Date	Grant W. Hart, Chair
Date	Bryan G. Peterson
Date	Ross L. Spencer

BRIGHAM YOUNG UNIVERSITY

As chair of the candidate's graduate committee, I have read the thesis of Michael Takeshi Nakata in its final form and have found that (1) its format, citations, and bibliographical style are consistent and acceptable and fulfill university and department style requirements; (2) its illustrative materials including figures, tables, and charts are in place; and (3) the final manuscript is satisfactory to the graduate committee and is ready for submission to the university library.

Date

Grant W. Hart, Chair
Chair, Graduate Committee

Accepted for the Department

R. Steven Turley, Chair
Department of Physics and Astronomy

Accepted for the College

G. Rex Bryce, Associate Dean
College of Physical and Mathematical Sciences

ABSTRACT

NON-INTRUSIVE TEMPERATURE DIAGNOSTIC

FOR A NON-NEUTRAL PLASMA

M. Takeshi Nakata

Department of Physics and Astronomy

Master of Science

A simple, non-destructive diagnostic for the temperature of a non-neutral plasma is desirable as plasma lifetimes increase and the confined species become more exotic. If the confinement system includes an isolated wall sector, the motion of the charges beneath that sector will result in a noise signal that can be directly related to the velocity distribution of the confined particles. Care must be taken to differentiate the resulting plasma signal from the instrumental noise spectrum and the strong signals from plasma oscillation modes. The theoretical basis of the relationship between the noise spectrum and the temperature as well as experimental results will be presented.

ACKNOWLEDGMENTS

I would like to thank my Lord God for all my blessings. Truly, his Hand is in every aspect of our lives. He is always there for each one of us. I would like to thank him also for the opportunity to be here at Brigham Young University at this time.

My family for all their patience and support. My mother Mami for her love and support. My father Otosan who has always supported me temporally throughout my life and continue to do so. My sister Hiromi and her family; Ryan, William, and Sierra for letting me have a place to escape when there seem to be no hope. My brother Tsuyoshi for his brotherly support and words of encouragement.

My friends who kept telling me that I can and made me laugh when I needed it. For my advisors, Dr. Hart and Peterson, for allowing me a chance to research and learn. It really has been an awesome, learning experience. My plasma research group for their encouragement and support. Lastly, but not least, the Department of Physics and Astronomy for all of their resources. And everyone else who has helped me throughout this journey.

Contents

List of Figures

1 INTRODUCTION AND BACKGROUND

One of the fundamental characteristics of a plasma and an important part of its dynamics is its temperature. In a non-neutral plasma, this measurement is usually done by dumping the plasma and measuring the velocity distribution. This method was developed by Eggleston while at UCSD in the early 1990's and in essence involves measuring how many electrons are energetic enough to escape the applied confinement potentials.[1] This entails "dumping" the plasma, or the lowering of one of the confining potentials slowly to allow the electrons escape to the detector, thus, losing the confined non-neutral plasma. It has since been desirable to find a non-destructive method to measure the temperature.

One non-destructive method that has been investigated is the use of the mode frequencies of the plasma to determine its temperature. This method investigated by Hansen at BYU was found to be not useful because of the weak dependence of the mode frequencies on temperature.[2] The mode frequencies were more dependent on the radial profile, which varied from shot to shot by several percent. According to Hansen, this change could translate to a temperature variation of 30%, making this method impractical.

It should be noted that all of these methods are actually measuring the parallel temperature. In a highly ionized magnetized gas such as a plasma, temperature related to the velocities in a direction parallel to the magnetic field is not necessarily equal to the temperature in the perpendicular direction. However, in most cases the

two temperatures equilibrate such that the parallel temperature is the same as the temperature of the plasma. We only specify here that it is parallel temperature we measure because there are cases where there is a difference. However, this research will be limited to the non-destructive measurement of the parallel temperature.

2 MALMBERG-PENNING TRAP

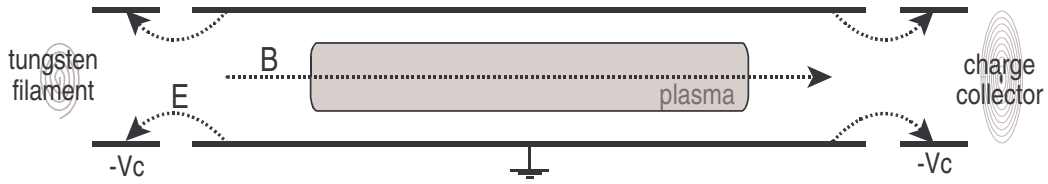

Figure 1: Electric and Magnetic fields in our Malmberg-Penning Trap

A Malmberg-Penning trap is used to confine our non-neutral plasma.[3] These traps have been found to have exceptional confinement properties for a nonneutral plasma. In these traps, the nonneutral plasma is radially confined by an applied axial magnetic field and axially confined by electrostatic potentials applied to ends of these cylindrical traps. In this subsection, we specifically describe our Malmberg-Penning trap at BYU. For the original description of this trap, I refer back to Hansen and Hart.[2, 4]

The Malmberg-Penning trap consist of hollow conducting rings which are enclosed in a cylindrical vacuum chamber. This vacuum chamber operates at an ultra high vacuum pressure of about 10^{-9} torr. The vacuum chamber resides in a solenoid which applies an axial magnetic field of about 700 gauss for radial confinement. Additional B_x and B_y saddle coils are used to correct for mechanical misalignments of the interior structure with the solenoid magnetic field and for the Earth's magnetic field. A voltage of -150 volts is applied to the end confining rings of this trap for axial confinement.

2.1 Confinement Theory

The axial confinement is assured by applying sufficiently high voltage to the end rings of this cylindrical trap such that

$$e|V_c| > e|\phi| + \frac{mv_{\parallel}^2}{2} \tag{1}$$

where V_c is the confining potential applied on the end rings, ϕ is the space charge potential of the plasma, m is the particle mass, and $v_{\parallel}$ is the parallel component of the velocity of the particles.

Radial confinement is assured by the conservation of total angular momentum of the plasma.

The total canonical angular momentum for a collection of charged particles in a Malmberg-Penning trap is

$$P_\theta = \sum_j [(mv_\theta r)_j - q_j B r_j^2/2] \tag{2}$$

where m, v_θ, r_j, q_j are respectively the mass, azimuthal velocity, radial position, and charge of the jth particle. For a pure electron plasma in this kind of trap, the mechanical term $mv_\theta r$ is much smaller than the dominant r_j^2 term such that they can be neglected. Now, by setting $q_j = -e$, the total angular momentum is just

$$P_\theta \sim \sum_j eBr_j^2/2 \tag{3}$$

By the conservation of this quantity and in the absence of external torques, this implies a constant mean square radius such that the plasma is restricted from expanding to the wall. However, in practice, because of field imperfections and

collisions with background gas, there are external torques which allow some of the plasma to reach to the wall by increasing the mean square radius. For a more complete description of the confinement theory, I refer to O'Neil's paper.[5]

2.2 Ring Description

The two end rings (Rings 1 and 9) are used to confine the nonneutral plasma. They are about 2.5 cm in length. The other 7 center rings (Rings 2 to 8) are used to detect and modify the plasma's behavior. They vary in length from 5 to 10 to 20 cm. Two of the 5 cm rings (Rings 4 and 8) are further azimuthally divided into four sections. They are used in the preparation of the plasma.

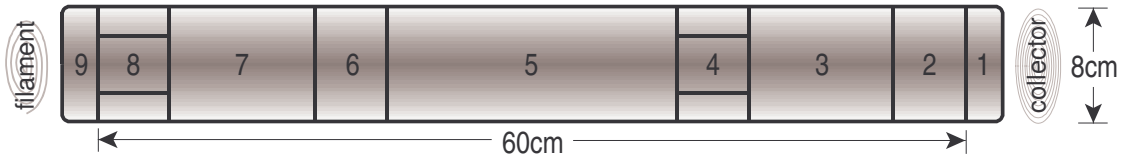

Figure 2: Schematic of our Malmberg-Penning Trap with ring numbers

On the first sectored ring (Ring 8), a static electric quadrupole field is applied to improve the reproducibility of the plasma from shot-to-shot. The top and bottom sectors are held at a negative voltage (0 to −40 V) while the left and right sectors are held at a positive voltage (0 to +40 V). This has a similar effect to applying a tilted magnetic field, such as Fine did in his experiments on the m=1 diocotron mode.[6]

When the column of plasma is shifted off-center, it rotates around the center

of the trap. This is called the m=1 diocotron mode. This m=1 diocotron mode is a negative energy mode. This means that to attenuate this mode, energy must be supplied to the plasma.[6]

On the second sectored ring (Ring 4), two opposing sectors are used to detect the m=1 diocotron mode. One of the other sectors is used to attenuate this mode by positive feedback.

The top and bottom sectors which detect this mode are connected to a differential amplifier. The output is used to attenuate this mode on the other sector. This keeps the diocotron mode in check such that it does not become unstable.[7, 8]

Each of these rings are electrically isolated from each other and from the vacuum chamber.

The inner radius of this trap is 4 cm and the total length between the confining rings is about 60 cm. This is therefore the approximate length of our electron plasma.

2.3 Plasma

Typical parameters for our electron plasma are: density $n \sim 10^7$ cm^{-3}, thermal energy of about $kT \sim 1$ eV, and for a 60 cm long plasma, an average axial transit time of about $\sim 1.5\ \mu s$.

This plasma is created by thermionic emission from a hot spiral tungsten filament. As electrons are emitted by this filament, the plasma continues to form until the plasma potential is equal to the filament potential. Consequently, the plasma

radius also increases until it matches the filament radius. This was first observed by deGrassie and Malmberg in the first experiments with a nonneutral plasma in cylindrical geometry.[9]

In their experiment, they found the filament potential Φ_k in the lowest order to have the following functional form:

$$\Phi_k = -V_b + V_f \frac{r^2}{R_k^2} \tag{4}$$

where V_b is the bias voltage applied on the center of the filament, V_f is the voltage drop across the filament, r is the distance from the axis of symmetry, and R_k is the radius of the filament.

They suppose the electron plasma potential Φ_s to be the same as the potential of a constant density electron gas in a grounded cylindrical conductor. This potential is

$$\Phi_s|_{r \leq r_p} = \frac{e}{4\pi\epsilon}(n\pi r_p^2)[1 + 2\ln(\frac{r_c}{r_p}) - \frac{r^2}{r_p^2}] \tag{5}$$

where r_p is the radius of the plasma, r_c is the inner radius of a grounded conducting wall, and n is the constant density.

By equating these potentials, $\Phi_k = \Phi_s$, they concluded that the electron plasma density n is proportional to the voltage drop across the filament, V_f, while the radius of the electron plasma, r_p, is determined by the filament bias voltage, V_b.

For our spiral filament, we apply a biased voltage V_b of about -60 volts, the voltage drop across our filament, V_f, is about 30 volts, and the radius of our filament, R_k, is about 4 cm.

2.4 Operations

This trap usually operates in a fill-prepare-experiment-dump cycle. In the dump stage we can measure the radial profile or the parallel velocity distribution of the electron plasma.

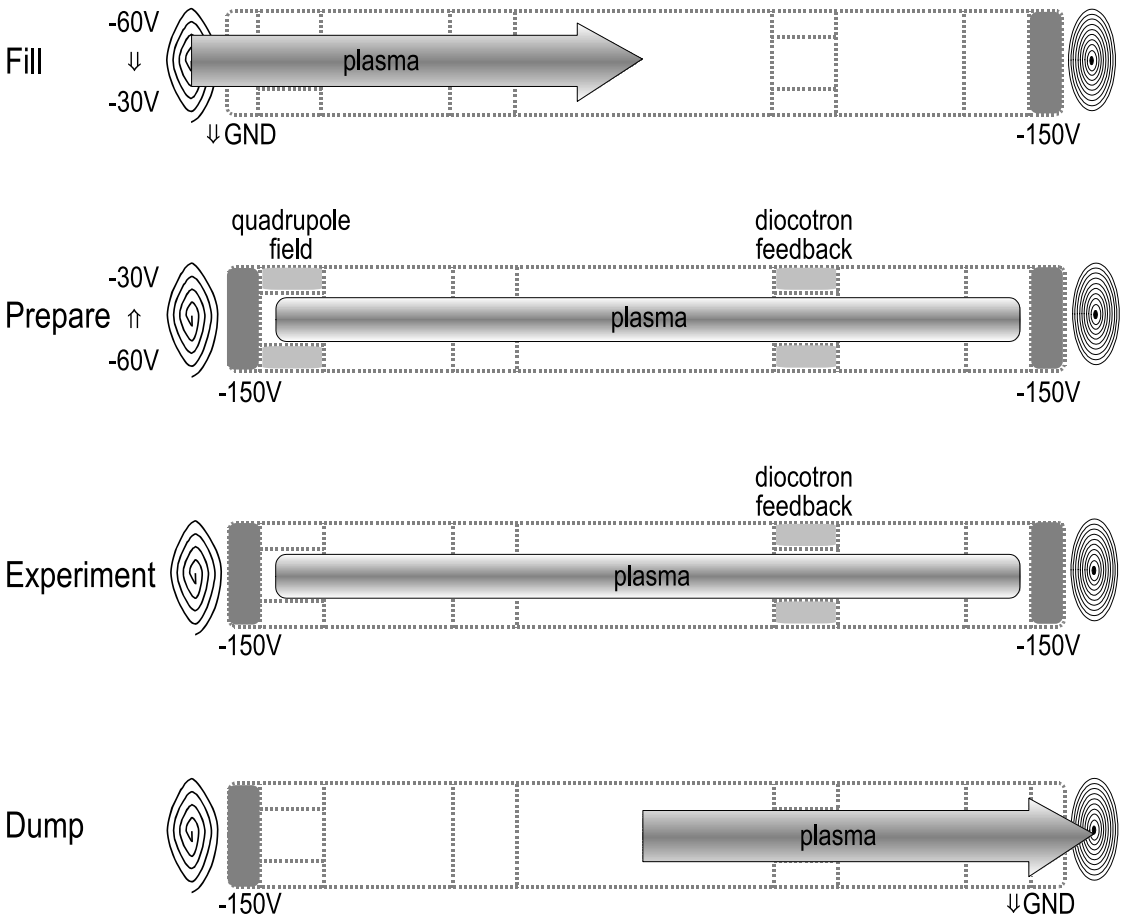

Figure 3: Timing Cycle Used in Our Experiment

Fill Stage To produce a pure electron plasma, first the filament is forward biased to emit electrons. Then, the first confinement ring's potential is lowered while the last confinement ring is maintained at a large negative potential to allow the

electrons to flow into the confinement region. Finally, this stage is completed when the first confinement ring's potential is raised back to its initial state and the filament is reverse biased to eliminate the thermionic emission of the electrons.

Preparation Stage After the plasma is formed and collected in this trap, a quadrupole field is applied on the first sectored ring which smooths the plasma and reduces shot-to-shot variation. On the second sectored ring, a diocotron feedback is also applied to maintain the stability of the plasma.

Experiment Stage After preparing the plasma for the experiment, the quadrupole field is turned off and the diocotron feedback may or may not be maintained, depending on the experiment to be performed. In our experiment, the diocotron feedback is maintained throughout this stage. Then the experiment is performed.

Dump Stage Finally, the last confinement ring's potential is lowered and the plasma is "dumped" onto 10 concentric rings. By measuring the voltage produced by the collected charge and knowing the capacitance of each of the rings, one can find how much charge is collected as a function of radius. From this measurement, one can find the plasma density's radial profile. The charge collected as a function of radius is related to the z-integrated density,

$$Q(r) = eA \int n(r) dz \tag{6}$$

where e is the charge of an electron and A is the cross sectional area of the ring. From this relationship, one can find the density of plasma as a function of radius,

$$n(r) = \frac{Q(r)}{eAL_p} \tag{7}$$

where L_p is the length of the plasma. In this calculation, we assume that the plasma is azimuthally symmetric. To obtain the actual plasma density's radial profile, one must do an equilibrium calculation using Possion's equation.[10]

Temperature Dump Stage To obtain the parallel temperature of the plasma, the "evaporative" technique developed by Eggleston is used.[1] The last confinement ring's potential is lowered slowly compared to the bounce time for a particle in the trap. Only the most energetic electrons from the axial center of the electron plasma escape onto the concentric rings at first while less energetic electrons are last to escape the potential well when the confinement voltage is lower. Thus, the escaped charge as a function of confinement voltage is a measure of the parallel velocity distribution of the electron plasma.

For a Maxwellian distribution of temperature, the charge escaped Q_{esc} is related to the parallel temperature $T_\parallel$ in the following way:

$$Q_{esc}(r, \phi_c) = qL \int dA' n(r') \operatorname{erfc}\left(\sqrt{\frac{E(r', \phi_c)}{kT_\parallel}}\right) \tag{8}$$

where $\int dA'$ is the integral over the collector area, L is the length of the plasma, $n(r')$ is the density of the plasma, and $E(r, \phi_c)$ is the the minimal electron kinetic energy required to escape over the confining potential ϕ_c. This kinetic energy has

the following form:

$$E(r, \phi_c) = q[\phi_c - \phi_p(r, \phi_c)] \tag{9}$$

where $\phi_p(r, \phi_c)$ is the plasma potential created by the remaining confined electrons. Both of these equations describe the evaporation method of measuring the parallel temperature of the plasma. The charge collected on our collector is related to the charge escaped Q_{esc} for a given confinement voltage ϕ_c.

3 THEORY

3.1 Review of Fourier Theory

Before moving onto the theory of our temperature diagnostic, we shall review some basic Fourier theory. This will assist us in better understanding the following discussion. For greater detail on this theory, I refer to Engleson and Witte.[11, 12]

The Fourier transform is a useful tool to transform a waveform in the time domain into the frequency domain.

$$F(\omega) = \int_{-\infty}^{+\infty} f(t)\, e^{i\omega t} dt \tag{10}$$

However, in actual time measurement, we do not have a continuous time function, so a discrete Fourier transform must be used to convert a sampled time signal into a sampled frequency form.

$$X(kF) = \sum_{n=0}^{N-1} x(n\Delta t)\, e^{i2\pi kFn\Delta t} \tag{11}$$

where k is the harmonic number, N is the number of samples, F is the spacing of the frequency domain samples, and Δt is the sample period in the time domain.

A sampled time waveform is basically the product of the sampling function and the actual time domain signal where the sampling function is just a series of delta functions spaced by a sampling period $\Delta t = 1/f_s$.

$$x(nT) = \sum_{n=-\infty}^{\infty} x(t)\, \delta(t - nT) \tag{12}$$

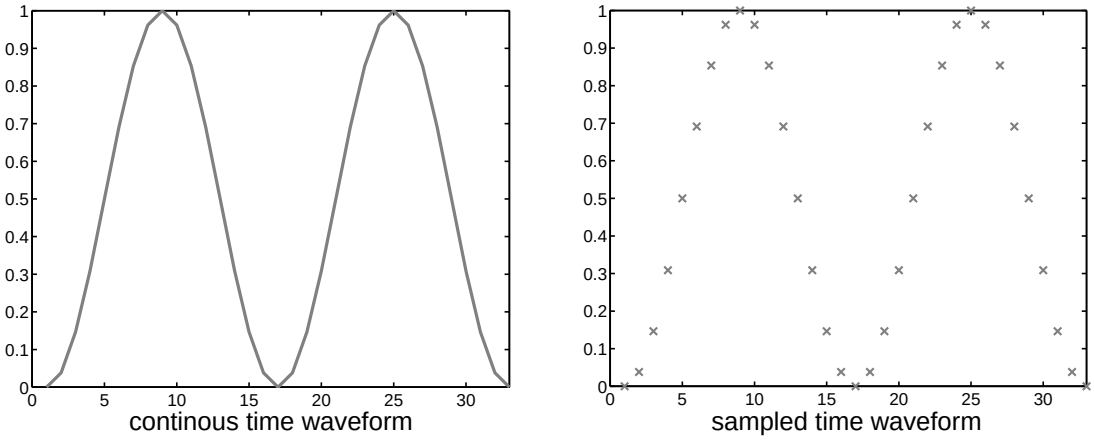

Figure 4: A Sampled Waveform

By using the convolution theorem, we get the original Fourier transform of the time domain signal.

The convolution theorem states the convolution of two time domain functions is the product of their individual spectra.[11] It also states that the convolution of two spectra is the product of two time domain functions.

$$\int_{-\infty}^{+\infty} f_1(\tau) f_2(t-\tau) d\tau \rightarrow F_1(\omega) * F_2(\omega) \tag{13}$$

$$\int_{-\infty}^{+\infty} f_1(\omega) f_2(w-\omega) d\omega \rightarrow F_1(t) * F_2(t) \tag{14}$$

If one of these time domain functions is the delta function like in our sampled time signal, the transform gives back the original time signal.

$$\int_{-\infty}^{+\infty} f(\tau)\delta(t-\tau) d\tau = f(t) \tag{15}$$

This is also true for the frequency domain such that we get back to the original frequency domain form of the sampled signal.

The sampling theorem states that the input signal must be sampled at least a rate twice the highest frequency present in the input signal. The minimum acceptable rate is called the *Nyquist rate*.[12]

$$f_s > 2f_{max} \tag{16}$$

Equation 16 illustrates this criterion where f_s is the frequency which one samples at and f_{max} is the highest frequency present in the input signal.

If the sampling theorem is violated, undesirable frequency components show up at frequencies other than their real frequencies which problem is known as *aliasing*. Thus, we desire to sample at a rate higher than the highest frequency present in our signal of interest.

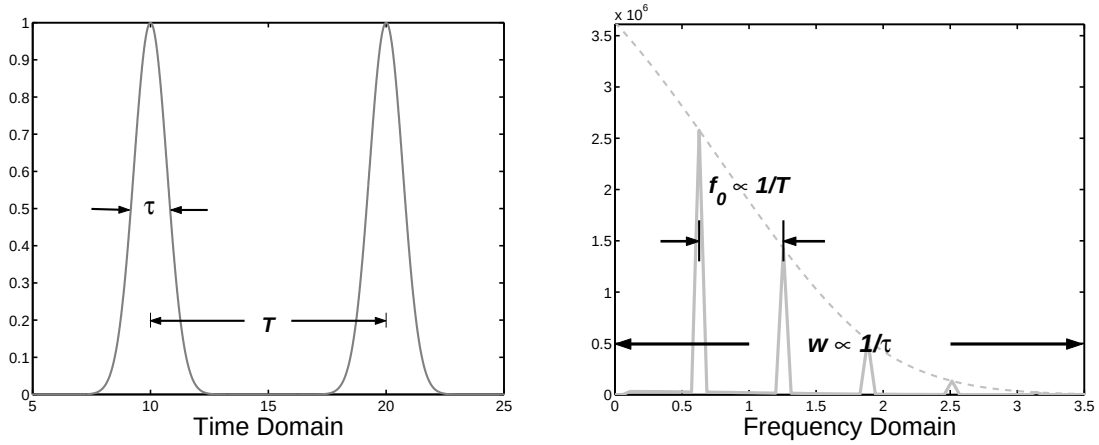

Figure 5: The Time Characteristics of Periodic Waveform

Let us consider a periodic waveform with two time characteristics like in Fig. 5. These time characteristics are the width of the pulses τ and the period between the pulses T. When one Fourier transforms a periodic waveform like this, the period

between the frequency peaks f_0 is proportional to the inverse of the period of the waveform $1/T$. While the width of the overall spectrum w is proportional to the inverse of the width of the pulse $1/\tau$.

The second thing to notice is that a sharp pulse in the time domain is a broad pulse in the frequency domain. The same holds true for the reverse case.

The third thing to observe from Fig. 5 is how the convolution theorem plays a role in Fourier transforming a signal.

Let as assume we have a function $F(t)$ like that in Fig. 5 in the time domain which is a product of one pulse $f(t)$ times a sampling function of a series of delta function $g(t - nT)$.

$$F(t) = \int_{-\infty}^{\infty} f(t)g(t - nT)dt \quad \text{where} \quad g(t) = \sum_{n=-\infty}^{\infty} \delta(t - nT) \tag{17}$$

When one Fourier transform this function $\mathcal{F}(F(t))$ using the convolution theorem, we obtain a function which is the product of the individual Fourier transforms of each of the functions $\mathcal{F}(f(t)) * \mathcal{F}(g(t))$.

$$\mathcal{F}(F(t)) = \mathcal{F}(f(t)) * \mathcal{F}(g(t)) \quad \text{where} \quad \mathcal{F}(g(t)) = \sum_{n=0}^{\infty} \delta(f - nf_0) \tag{18}$$

In our example, it is the Fourier transform of one pulse times the Fourier transform of a series of delta functions. This can be observed in the frequency domain, by noticing that the envelope is the Fourier transform of one pulse, while the spikes have the same interval as the Fourier transform of a series of delta

functions. And the amplitude of the one pulse Fourier transformed (the envelope) is proportional to τ/T.

3.2 Noise Spectrum Theory

The One Particle Case

We use an isolated ring that may or may not be segmented to measure the signal of interest. As an electron passes underneath the ring, it induces a charge in that ring, as a function of time. This signal is measured as a pulse in our detector.

The amplitude of the pulse is related to the charge that is induced on the ring by an electron. This amplitude does not change with velocity.

In contrast, the width of this pulse is a function of the velocity of the electron under the ring. As the velocity of the electron under the ring increases, the width of the pulse decreases.

On the other hand, the shape of the pulse is determined by how close the electron is to the isolated ring wall. As the electron nears this wall, the shape of the pulse changes from a rounded edge pulse to a square edge pulse. For our electron plasma, most of the electrons are far from this wall, so the shape for each of the pulse is a smooth one.

In addition, the length of the detector influences all of these parameters as illustrated in Fig. 6. The amplitude and width of the pulse increases with the length of the detector. However, when the length of the detector is much greater

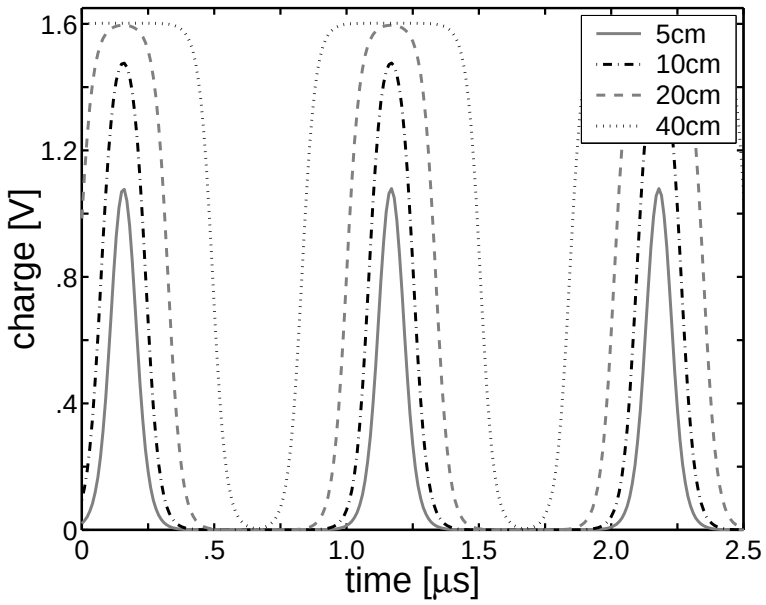

Figure 6: How the Pulse changes with Detector Lengths

than its diameter, as is the case for the 40 cm ring, the amplitude of the pulse remains a constant, the width continues to increase with length, and its shape goes from a round edge to a square edge.

By Fourier transforming this signal, we find that the frequency spectrum is also a function of the velocity of the electron. As the velocity of the electron increases, it lowers the transit time of the electron under the ring which translates to higher frequencies in the corresponding spectrum.

The Many Particle Case

For a collection of electrons like in our plasma, this velocity is the thermal velocity of the electrons which is related to the temperature of the plasma in that direction. In this case, the direction is parallel to the confining magnetic field.

$$v_{th} = \sqrt{\frac{2k_B T}{m_e}} \propto l_{ring} f \tag{19}$$

Equation 19 demonstrates how the frequency is proportional to the square root of the parallel temperature $\sqrt{T_\parallel}$.

The spectrum for the many particle case is both a function of the length of the detector and the parallel temperature. As the parallel temperature increases, the spectrum shifts toward higher frequency. As the length of the detector increases, the overall width of the spectrum decreases.

The amplitude of this spectrum is influenced by both the parallel temperature and number of particles in the plasma. As the parallel temperature increases, the amplitude increases about $T^{-\frac{1}{4}}$. As the number of particles increases, the amplitude increases as $\sqrt{N}$.

In this collection of particles, each electron contributes in an incoherent manner to the induced charge. In consequence, the contribution to the spectrum by particles of velocity v scales as $\sqrt{N}$, where N is the total number of electrons under the ring at a particular thermal velocity. While the time domain signal is incoherent, the frequency domain signal adds up as $\sqrt{N}$.

This signal is just the shot noise of the plasma current passing under the ring. It is the fluctuation signal, or the noise on top of the overall charge signal in the time domain. Thus, by examining the frequency spectrum of this signal, one can determine the parallel velocity distribution and therefore the parallel temperature of the electron plasma. Typical times for an electron in a 1 eV plasma under a

ring of 20 cm is $\sim 0.5\mu$s which implies a typical frequency of $\sim$2 MHz.

3.3 Simulation

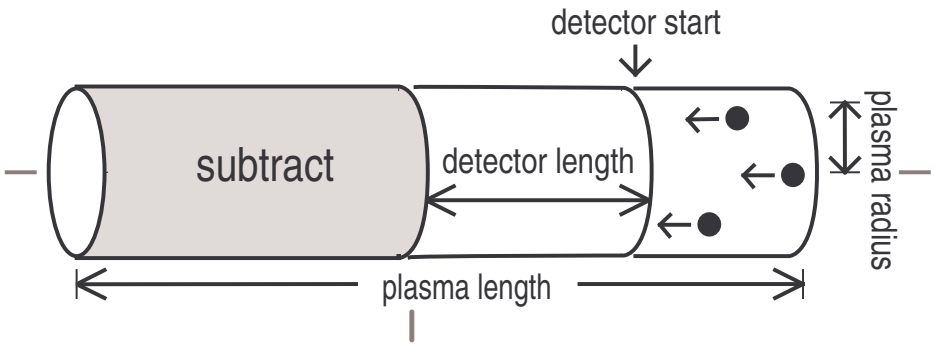

Figure 7: Conceptual drawing of simulation calculation.

To gain an understanding of how the temperature is related to this noise signal, we created a simple simulation where the particles do not interact with each other.

First, we began by solving for the induced charge due to a charged particle in a half infinite grounded cylinder using a Green Function like this:

$$Q(z) = \int \rho(r', z')\ G_D(z, r', z')\ 2\pi r' dr' dz' \tag{20}$$

$$\text{where } G_D(z, r', z') = \sum_{n=1}^{\infty} \frac{J_0(k_{0n} r') e^{-k_{0n}(z-z')}}{k_{0n} J_1(x_{0n})} \tag{21}$$

where $k_{0n} = \frac{x_{0n}}{a}$ and x_{0n} are the roots of $J_0(x_{0n})$ and a is the radius of the detector. We also restrict ourselves to the azimuthally symmetric case.

From Fig. 7, we first calculate the induced charge from where the detector starts. Then, we calculate the induced charge from where the detector length ends. Finally, we subtract these two quantities to obtain the induced charge on

our simulated detector (a ring) from a charged particle.

Because this Green function calculation takes about 200 terms to converge reasonably, we calculate this function once. Then, we save it as a lookup table of (r, z) in which we interpolate to get the induced charge for the rest of the particles.

Next, we fill this grounded cylinder with a randomized Maxwellian distribution of charged particles. We then move them in time knowing each of their velocities for a sample time. At each time, we calculate the charge induced on the ring due to each particle. As each particle reaches the end of the plasma, it elastically bounces off our simulated confining wall.

Consequently, we obtain the induced charge on this cylinder as a function of time. We then subtract the average value of this signal, to obtain just the fluctuations in the time signal.

Finally, we FFT this time signal to obtain a spectrum. We then average a number of spectra to ultimately obtain our theoretical noise spectrum.

Typical parameters for this simulation were 1000 particles, 40 ns sample time, 1024 samples, detector start at 10 cm from the origin, 20 cm detector length, a plasma radius of 2 cm, a plasma length of 60 cm, a plasma temperature of 1 eV, and we average about 50 spectra.

These simulations were both done for the charge induced in the ring Q and the current flowing to the ring $\frac{dQ}{dt}$. The width of these spectra are proportional to the average thermal velocity, thus related to the temperature. In Fig. 8, one can see that as temperature of the plasma is increased, the width of the spectrum increases

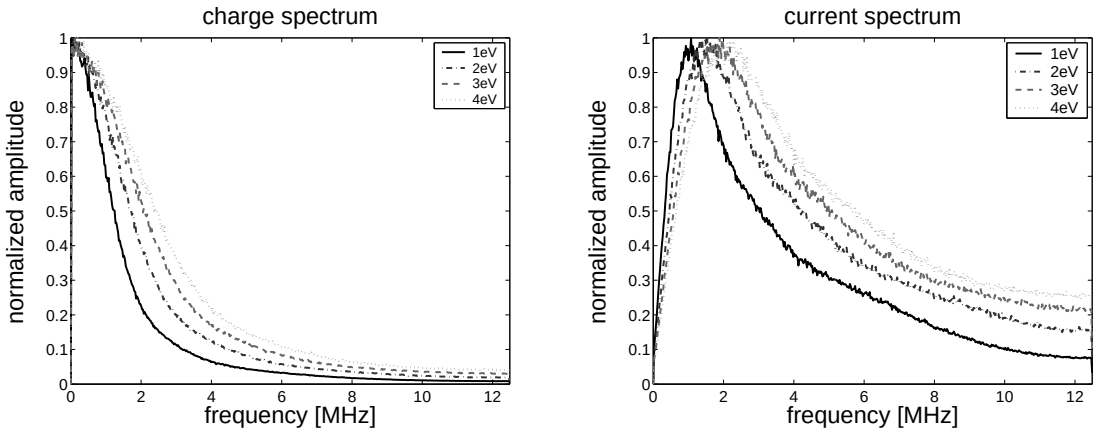

Figure 8: Simulated Spectras of a plasma under a 20cm ring.

accordingly. One also finds that this width is easier to determine in the current measurement than the charge measurement. Both of these spectra's amplitude has been normalized.

Another thing to notice from this simulated spectrum is the fact that there are no collective effects present in the spectrum because these particles are non-interacting particles. Of course, in our experiment, the electrons are interacting and collective effects such as mode oscillations in the plasma are present in our measured spectrum.

3.4 Analytical Fitting Attempts

In developing the theory for this measurement, we attempted to find an analytical fit for a charge going under a ring.[13, 14] A gaussian, tanh, square, and erf pulses were used to try to fit to the simulation. The following forms were used for the

gaussian, tanh, and erf pulses:

$$\begin{aligned} &A * \exp(-(x/w)^2) && \text{gauss form} \\ &A * (\tanh((x+c)/w) - \tanh((x-c)/w)) && \text{tanh form} \\ &A * (\text{erf}((x+c)/w) - \text{erf}((x-c)/w)) && \text{erf form} \end{aligned} \tag{22}$$

where A is the amplitude, w is the width of these pulses, c is controls the curvature of the erf and tanh pulses.

It was found that the tanh was the best for the 10 cm and 20 cm ring, while, the gaussian did fairly well in fitting the 5 cm ring. The square pulse is also fairly good in fitting the case when the particle is near the cylindrical wall. However, when each of these analytical pulses were Fourier transformed, each did not quite correspond to the simulated spectrum. Nevertheless, it gave us some insight to understanding the signal of interest.

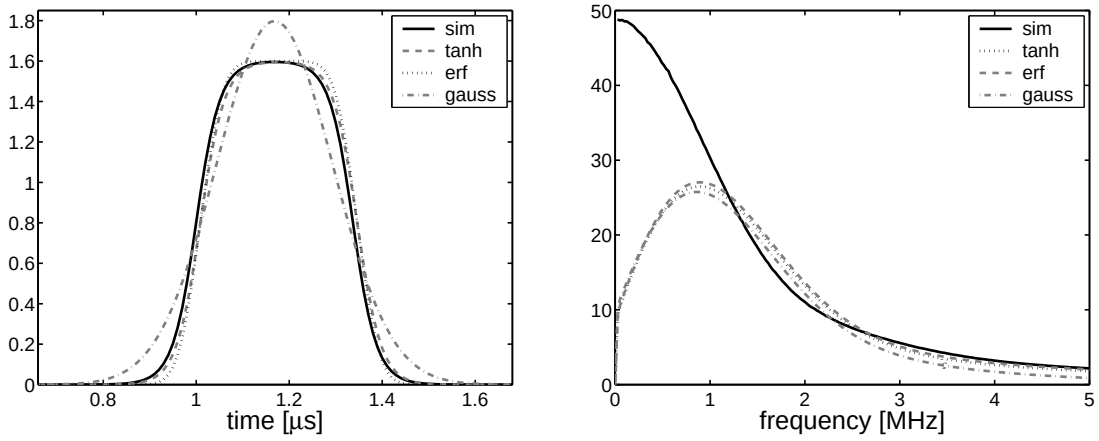

Figure 9: Simulation vs. Analytical for a 20 cm ring

From Fig. 9, one can see that the tanh pulse fits the best to the simulation of a 20 cm ring in the time domain while in contrast the gaussian is a terrible fit. How-

ever, in the frequency domain, all the analytical fits are poor in comparison with simulation. One finds that all the analytical fits do not have the right curvature to match the simulation.

In conclusion, it appears that the signal from an electron plasma can not be reliably represented by any simple analytical function. However, further research in better understanding this theory may allow us to find a simple analytical fit which can be applied to find the simulated noise spectrum.

4 EXPERIMENTAL TECHNIQUE

4.1 Noise Temperature Diagnostic

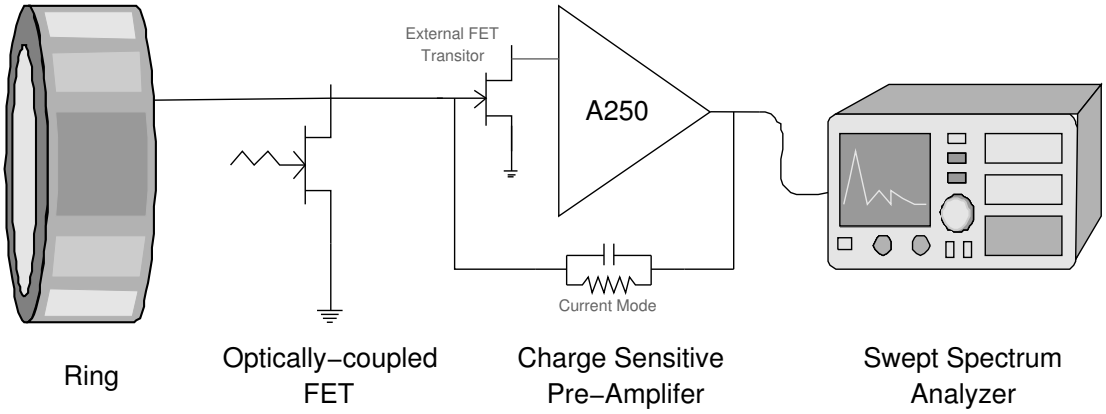

Figure 10: Noise Temperature Diagnostic

Fig. 10 illustrates our basic setup for the noise spectrum temperature diagnostic. It basically consists of a ring, a charge sensitive preamplifier, and a swept spectrum analyzer.

Ring

To measure the noise spectrum, we use an isolated ring on our trap. As charges moves beneath the ring they induce a noise signal that is directly related to the velocity distribution of the confined particles. This noise signal depends on both the position and the length of the ring.

After some exploration of different rings, we decided to use our center 20 cm

ring on our trap. This ring is our longest ring which, in our simulation, we find to result in the largest signal in amplitude. Its position in the center is also optimal in that it is insensitive to the $n_z = 1$ normal mode which usually is found in our temperature sensitive range of 1 to 3 MHz for our plasma parameters.

Charge Sensitive Preamplifier

When we fill or dump our plasma from the trap, a large voltage pulse is induced on our ring. This pulse saturates our preamp and once the amplifier is saturated, it takes more than the lifetime of our electron plasma to return to normal operation. In order to not saturate our amplifier while this occurs, we use an optically coupled FET transistor connected between the ring and the ground. This FET is only turned on when data is not being acquired.

To permit optimization of this preamp, the input field effect transistor has been left external to allow it to be cooled to reduce noise. However, in our application of this preamp, it was utilized in its normal configuration.

This amplifier (an AmpTek A250) can be configured either to produce a signal proportional to the charge on the ring or the current flowing into it. The current can be detected by connecting a feedback capacitor and a large resistor to the preamplifier, thus, making a differentiating circuit which measures signals proportional to the current flowing through the ring.

Spectrum Analyzer

Since there is significant instrumental noise in the frequency range of interest, we must subtract that from our signal. To do this we use a spectrum analyzer to acquire the spectrum with plasma and the spectrum without plasma under the ring.

This acquisition can be done in two ways. One is to scan the range of interest which in our case is about 0 to 10 MHz in one shot. However, we then take multiple shots to get a time history of our signal. The resolution of this time history is limited by the spectrum analyzer's sweep time. Thus, our best time resolution is about 20 ms. Under some circumstances the plasma can change significantly in that time.

The other method is to set the spectrum analyzer to "span zero". In this mode, the spectrum analyzer looks at one frequency for the entire sweep time. This shows us how the amplitude of the signal varies in time for one frequency. It basically is an AM radio receiver tuned to one frequency. The biggest drawback to this method is that we need to take a new shot (plasma) for each frequency. Because of shot-to-shot variability, we need to average 5 traces at each frequency.

From both of these methods, we can obtain how the plasma noise spectrum evolves with time. Thus, our data set is a function of time, frequency, and amplitude. Of course in postprocessing this data, we usually look at the spectrum at one time.

Postprocessing

Our first step in this postprocess is to subtract the spectrum with plasma from the spectrum without plasma. Then we take into account the frequency response of the charge sensitive preamplifier by normalizing our spectrum from its response which we measured earlier.

Next, we fit our data to a spectrum from the simulation for a 1 eV plasma for a 20 cm ring. To do this, we first eliminate frequency bands which have the mode frequencies. For our spectrum, these frequency bands are $0 \sim 1.24$, $2.74 \sim 5.02$, and $6.04 \sim 8.02$ MHz.

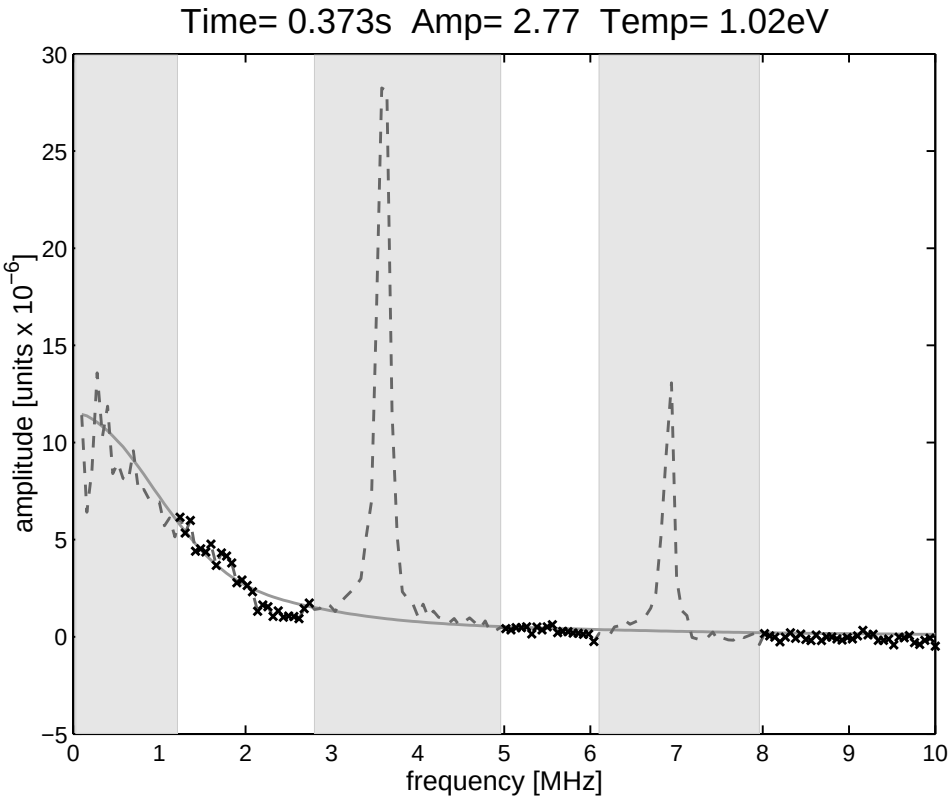

Figure 11: 5 Oct 2000, #1 data fitted to our simulation

Fig. 11 illustrates how our data is fitted to our simulated spectrum. We first eliminate the shaded frequency bands from the raw spectrum (the dashed curve), to obtain the spectrum used to fit our data. This spectrum, the 'x' data points is then use to fit to our simulated curve, the solid dark gray line.

Then, we use a nonlinear least squares algorithm to fit to the spectrum from the simulation. In the algorithm, the number of particles N and the parallel temperature $T_{\|}$ are used as adjustable parameters to fit to the data spectrum.

The minimizing function S for this algorithm is:

$$S = \sum_i \left[y_i - \frac{\sqrt{N}}{T^{\frac{1}{4}}} \mathcal{M}\left(\frac{x_i}{\sqrt{T}} \right) \right]^2 \tag{23}$$

where (x_i, y_i) is our data spectrum: frequency and amplitude; (N, T) are adjustable parameters: number of particles and temperature; and $\mathcal{M}$ is our theoretical spectrum from our simulation for a 1 eV plasma under a 20 cm ring.

This minimizing function illustrates how the amplitude and width of a 1 eV spectrum scales with the number of particles N and the parallel temperature $T_{\|}$. The amplitude goes as the square-root of the number of particles $\sqrt{N}$ over a weak temperature dependence of $T^{\frac{1}{4}}$. The width which is related to the thermal velocity v_{th} of the plasma is proportional to the square root of the parallel temperature $\sqrt{T_{\|}}$. Thus, we are able to use a 1 eV plasma spectrum for a 20 cm ring from our simulation to find how the parallel temperature and the number of particles evolve in time.

Analysis Tools

Both the number of particles and temperature parameters from the noise spectrum can be compared to the standard methods of obtaining these parameters from our nonneutral plasma.

For the number of particles, we integrate the radial profiles of our nonneutral plasma to get the actual number of particles. We obtain these radial profiles by dumping our electron plasma unto our concentric rings at the end of our Malmberg-Penning trap.

To compare this number of particles from the standard method to our noise spectrum parameter we use their time averaged values as a normalization constant for the noise spectrum. This normalization constant is $\frac{<N_{rp}>}{<N_{ns}>}$ where the subscript rp is the radial profile value, the subscript ns is the noise spectrum value, and the brackets means their time averaged values. By multiplying our noise spectrum parameter by this constant, we can relate this noise spectrum parameter to the standard method of integrating the radial profiles to obtain the number of particles in our nonneutral plasma.

For the parallel temperature, we use the standard evaporation method which we discuss in more detail in the next subsection for comparison to our noise spectrum parameter.

4.2 The Standard Evaporation Method

We use Eggleston's simple method [1] to get the parallel temperature for comparison. For this measurement, we slowly ramp the confinement voltage toward ground by applying a resistor between the confining ring and the driving supply. This means that as we ground the ring the voltage decays with a long RC time of about ~ 1 ms.

Electrons with sufficient parallel energy to escape the confinement region escape to the charge collectors at the end. Most of these electrons are from the center of the plasma which has the most negative space charge potential and lowest confining potential. Thus, we measure the charge escaped Q_{esc} versus the confining potential at the center ϕ_c.

For a long confining ring, the confining potential at the center ϕ_c is approximately the confining potential on the ring V_c. However, we have a short confining ring of about 2.5 cm. We take this into account by making a calculation of the minimum potential at the center of the ring for a given confining potential on the ring wall. This potential slightly changes when a plasma is present but it is near the calculated potential. For our geometry we divide our ring confining potential V_c by 2.456 to find the plasma potential ϕ_c at the center of our electron plasma.

Then, we fit our data of Q_{esc} vs. ϕ_c to the tail end of a Maxwellian distribution. As it was noted by Eggleston,[1] the slope of this curve in a y-axis log plot is related

to the parallel temperature in the following way:

$$\frac{d\ln(Q_{esc})}{d(q\phi_c)} = \frac{-1.05}{kT_{\|}} \tag{24}$$

Equation 24 was derived from the model equation 8 which describes how the charge of escaping electrons Q_{esc} is related to the parallel temperature $T_{\|}$ of the plasma.

From equation 24, we easily can obtain the center parallel temperature $T_{\|}$ of the plasma. One major advantage of this method is that it can be done with a single shot. In actuality, we average about 5 shots because of shot-to-shot variability to get the temperature for comparison to our noise measurement.

4.3 Swept Spectrum Analyzer

Why a swept spectrum analyzer is used?

There are two ways to get our noise spectrum from the ring of our trap. One is to acquire a time trace of our signal and then Fast Fourier Transform that trace. The other is to use a swept spectrum analyzer.

Initially, we used a LeCroy Oscilloscope to obtain a trace and FFT it. We soon discovered that one of the characteristics of our system was that we had 12 to 17 MHz noise that dominated our spectrum. This noise originates inside our vacuum system and seems to be due to resonances in the rings and cables. This noise limits the resolution of our signal of interest to the point that we could not see it. We also have normal mode plasma oscillations that limit our resolution.

The main problem with this method of acquiring our spectrum is that the

oscilloscope is limited by the analog-to-digital conversion resolution of 8 bits. When the other signals are full scale on the oscilloscope, the signal we are looking for is smaller than the bit size. Having more bits would theoretically solve the problem, but we did not have such devices. Thus, we decided to use a spectrum analyzer to obtain our noise spectrum.

How a Spectrum Analyzer Works

A swept spectrum analyzer operates on the principles of a relative frequency movement between the signal and the filter. This process is describe by the convolution theorem. In the spectrum analyzer, $f(\tau)$ is the stationary filter while $f(t-\tau)$ is the sweeping frequency signal. Thus, using a spectrum analyzer we can get the spectrum of an input signal as long as we have a narrow enough stationary filter.[11]

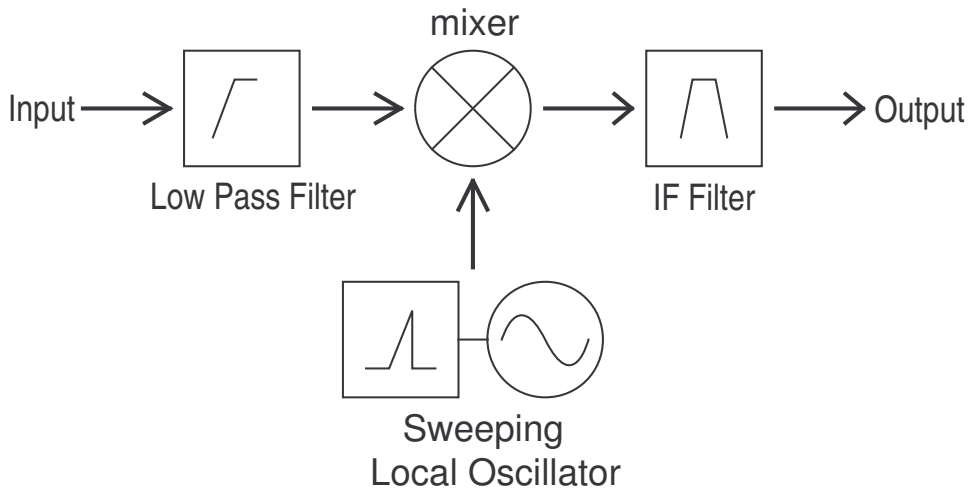

Figure 12: Basic Spectrum Analyzer Block Diagram

Figure 12 illustrates how a spectrum analyzer works. First, the input signal (also known as the *RF signal*) goes through the *low pass filter* which has the same function as an anti-aliasing filter does in a FFT in an oscilloscope. It blocks unwanted higher frequency components from getting downstream to our detector.

Next, it goes through the *mixer* where the input signal is multiplied by the *sweeping local oscillator (LO)*. The local oscillator generates an oscillation frequency that is swept by a ramp generator. This allows us to adjust the range of frequencies we can scan (also known as the *span*).

In consequence of this multiplication, the input signal in frequency is shifted to the center of the IF filter. In effect, the IF filter always remains tuned to the same center frequency which is the *intermediate frequency (IF)*.

To better understand this multiplication, let us say we have an input signal which is a cosine:

$$v_{rf}(t) = Acos(2\pi f_{rf} t)$$

and the local oscillator which is another cosine

$$v_{LO}(t) = cos(2\pi f_{LO} t)$$

Then the output of the mixer is

$$v_{IF} = Acos(2\pi f_{rf} t)cos(2\pi f_{LO} t)$$

which is equivalent to

$$v_{IF} = \frac{A}{2}[cos(2\pi(f_{rf} + f_{LO})t) + cos(2\pi(f_{rf} - f_{LO})t)].$$

Thus, the intermediate frequency f_{IF} has components at both the sum and difference of the LO frequency f_{LO} and the input frequency f_{RF}. Another thing to notice in this result is the output from the mixer has an amplitude, A, simply related to that of the input signal.

Finally, since the LO frequency changes with time, the RF frequency that gets mapped into the IF filter also changes with time. This results in a spectrum of the RF signal in real time which we detect with a detector. This IF filter is the *resolution bandwidth filter* of our spectrum analyzer which is used to look at one frequency at a time.

For more information about how spectrum analyzer works, I refer to Engleson and Witte.[11, 12]

How a Spectrum Analyzer displays Signals

To illustrate how an input signal is displayed by the spectrum analyzer, I used Engleson's figure,[11] for the basis of Fig. 13. The layout of this figure has a similar organization to that of Fig. 12. We have an input signal (top-left) consisting of two discrete frequencies that mixes with the local oscillator (bottom-left). The resulting mixed signal (top-middle) then goes through an IF filter (top-right) which is finally displayed on the CRT display (bottom-right).

In this figure, we have an input signal with two frequency components. The local oscillator output is a sawtooth signal that sweeps the range of interest where S is the span of the spectrum analyzer and T_s is its sweep time. In the IF filter

input, one can see that the IF filter is where the resolution bandwidth BW_{res} is set. Thus, this figure illustrates how an input signal with two frequency components are displayed on a spectrum analyzer.

Sweep Time Limitation

The fundamental limitation of a swept spectrum analyzer is its sweeping time. The sweeping time T_s is inversely proportional to the resolution bandwidth BW_{res}. Thus, for better resolution, one needs to sweep slower. This limitation make sense in the fact that the IF filter needs time to respond to the changing signal. If the signal is swept too fast, the IF filter only gets a sense of what the spectrum looks like and not the actual spectrum.

When we first began the acquisition of our plasma spectrum, we first started by just scanning the range of interest of 0 to 10 MHz at our fastest sweep time of about 20 ms. The result was a spectrum that seemed to have artifacts that demonstrated that we were not sweeping fast enough. For example, the mode oscillations lines in our spectrum were asymmetrical. A more fundamental concern was that within the sweeping time, the parallel temperature of our plasma may be changing. Thus, we concluded that we needed a better resolution at each frequency to get a reasonable signal to noise ratio to measure the temperature from our plasma noise spectrum.

Based upon the preceding considerations, we decided to acquire our spectrum by setting our spectrum analyzer to zero span. In effect, this gives us the best resolution possible for a given amount of sweeping time. However, one of the

drawbacks to this method is that we need to take a new shot (plasma) for each frequency. In consequence of using this method, our acquisition of data became a long process and not a short process as we had hoped.

Later on, we looked at how the temperature of our plasma changes with time. We observed that within the sweeping time of the spectrum analyzer, the parallel temperature of our plasma does change. Thus, zero span is the method used to get the parallel temperature from the plasma noise spectrum.

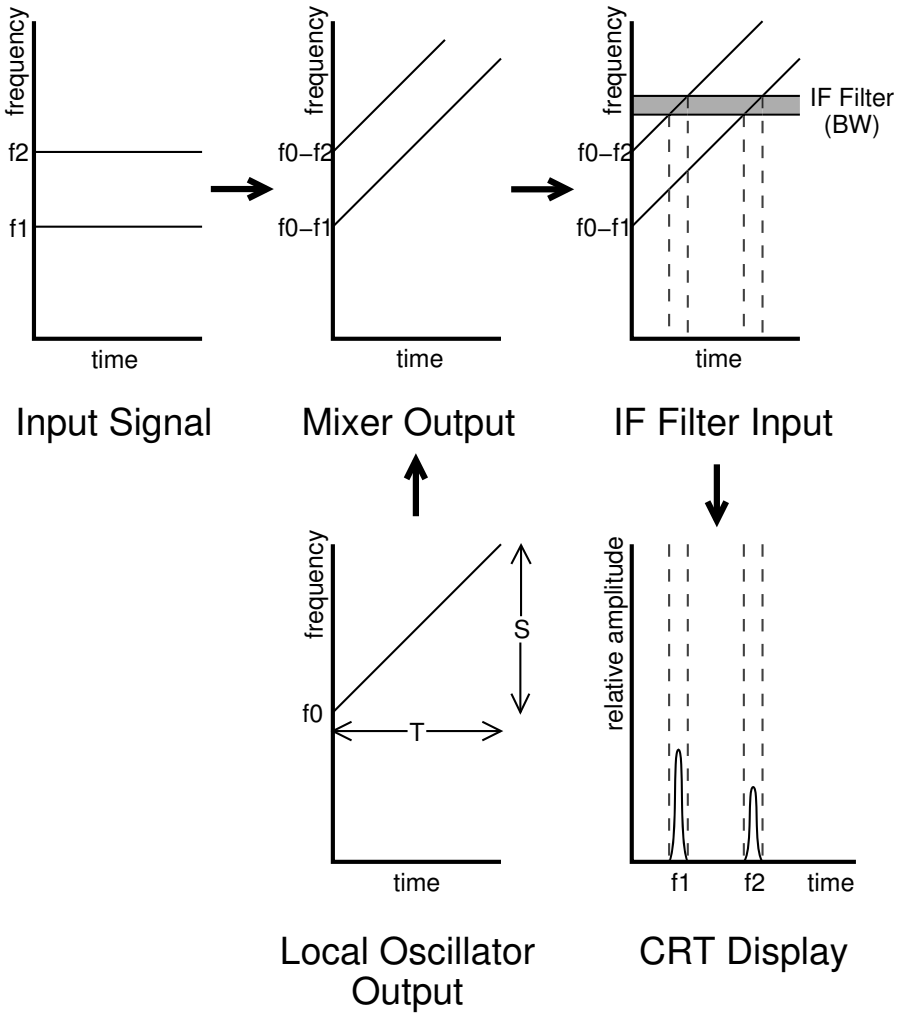

Figure 13: How input signals are displayed in a Spectrum Analyzer

5 EXPLORATION

5.1 The Search for the Right Ring

To find a non-destructive parallel temperature diagnostic we began with the exploration of which ring would be best as our detector. From the simulation we learned that the region of the spectrum that is most sensitive to the temperature is 1 to 3 MHz. Our objective was to find an optimal ring for this region.

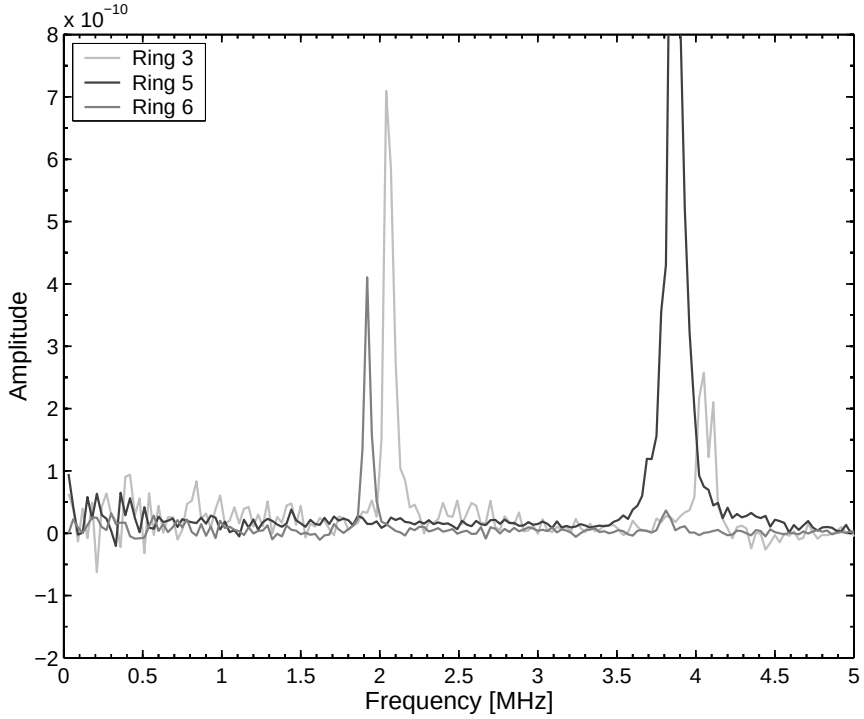

Figure 14: Different Rings

Fig. 14 illustrates our findings of how the spectrum looks like for rings 3, 5, and 6. These rings are sensitive to different axial plasma mode oscillations which are known as Trivelpiece-Gould (TG) modes. In these rings we only observed the first

2 TG modes. These are the $n_z = 1$ "slosh" mode about 2 MHz and the $n_z = 2$ "breathing" mode about 3.75 MHz.

Ring 3 (10 cm in length) is sensitive to both of these TG modes. On the other hand ring 5 (20 cm in length) and ring 6 (5 cm in length) are both exclusively sensitive only to one of these modes. Ring 6 is weakly sensitive to the "breathing" mode. For our interest region of 1 to 2 MHz, ring 5 is the ideal ring to use to measure our noise spectrum.

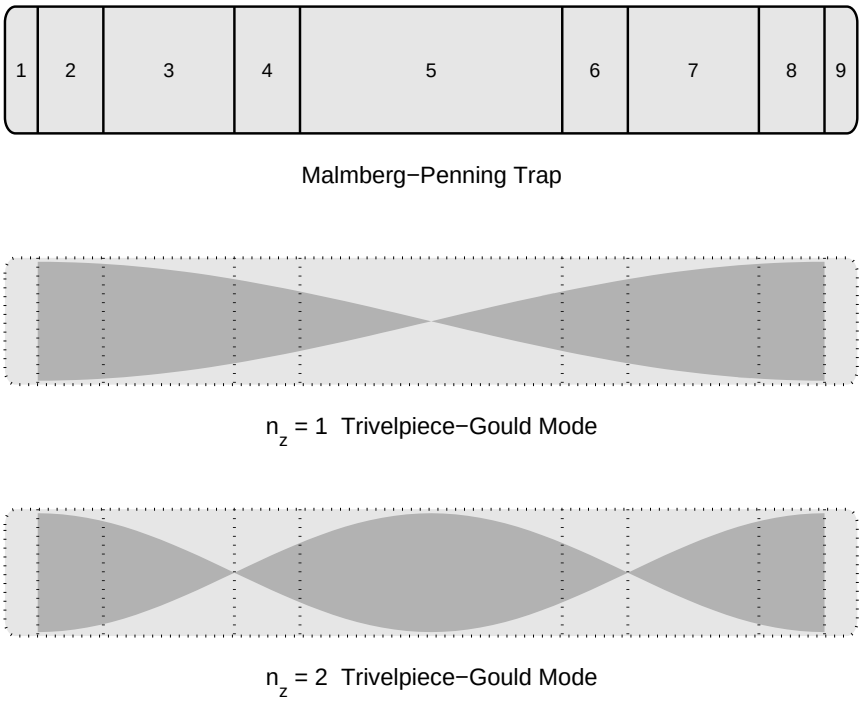

Figure 15: Trivelpiece-Gould modes

The sensitivity of these rings for a given TG axial mode depends on both the position and length of the ring. When we detect these TG modes in our ring the density perturbation is integrated over the length of the ring. Thus we are

insensitive to TG modes which have a node in the center of the detector. In contrast, the greatest sensitivity is gained when our detector length covers one node to another node for a given TG mode.

Fig. 15 illustrates a simple diagram as how the first 2 TG modes would be spatially aligned in our electron plasma. A centered ring (like ring 5 in our Malmberg-Penning Trap) would be insensitive to the first TG mode but be sensitive to the second TG mode. From these considerations one can see why each ring is sensitive or insensitive to particular TG axial modes.

Thus ring 5 is not only insensitive to the $n_z = 1$ "slosh" mode but also all subsequent odd TG modes. It also is our longest ring (20 cm in length) making it optimal in our noise spectrum measurement because, as observed from the simulation, the amplitude of the signal of interest scales with the length of the detector.

5.2 Experiments with Change of Temperature

Our next exploration was to see what happens when we change the plasma temperature. We started with an attempt to heat our electron plasma. This was done by driving a sinusoidal voltage signal of about 1 V at 1 to 3 kHz on one of our end rings such as ring 1 or ring 9 of our Malmberg-Penning trap (see fig. 15) which normally is set at a DC confining potential.

Fig. 16 illustrates how our plasma responds to a sinusodial voltage on our end ring. It generates other TG modes not present in our initial equilibrium state.

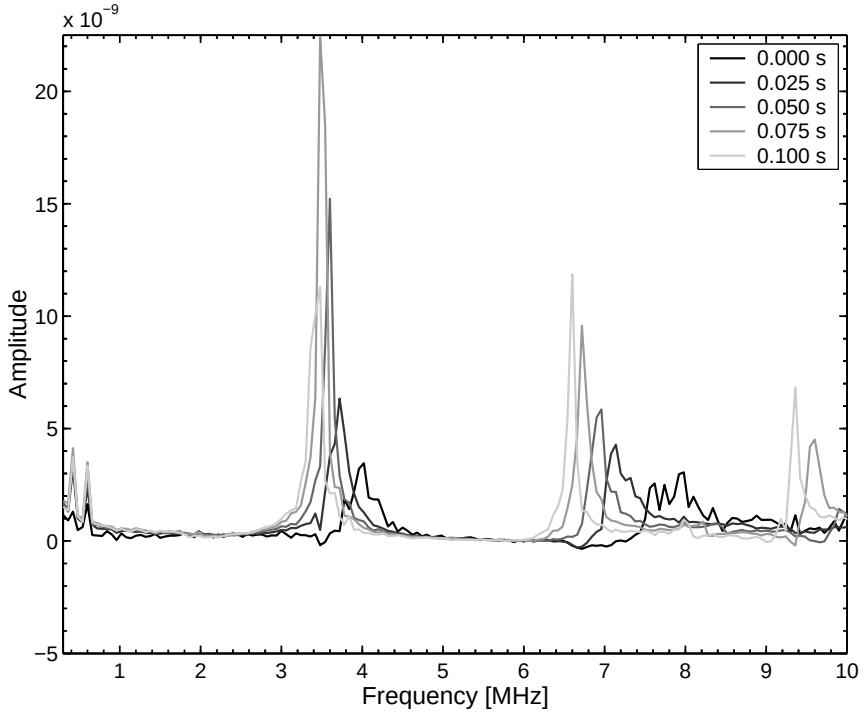

Figure 16: The Heating Attempt

Initially we only observe TG modes at 3.75 MHz and 7MHz for our ring. After applying a sinusodial voltage on our end ring we observe two more TG modes at about 0 to 1 MHz and 9 to 10 MHz. Thus making it difficult to use our noise spectrum method to get a parallel temperature because of the oscillations at 0 to 1 MHz.

When we first analyzed this spectrum we assumed that we were heating our plasma, but an closer inspection we realized that this plasma is cooling in time. Fig. 16 shows how the TG modes peaks are shifting down in frequency and getting narrower with time. These characteristics which we discuss later is consist with an electron plasma cooling with time.

In consequence of this we decided to just observe the cooling of the plasma to its thermal equilibrium state. This is accomplished by just letting the electrons radiate cyclotron radiation and letting them collide with neutral atoms that are still present after the electron plasma is formed. As we discuss later, as the plasma expands, the outer region of the plasma is heated, the final state is attained when the expansion heating is balanced by cooling.

5.3 The Current Method Attempt

In our simulations we found one major characteristic in the current spectrum was a hump around 1 to 2 MHz in the spectrum. As temperature increases in our plasma, the hump in the spectrum moves toward higher frequency. Because of this distinct feature, we decided to look at first the current noise spectrum on the ring of our trap.

However, once we obtained this current spectrum, we found that there was no sign of a hump in our spectrum in the 1 to 2 MHz range. Fig. 17 illustrates how the instrumental noise level dominates in this spectrum such that one can not determine if there is a signal or not. Thus we decided to use the charge spectrum to see if we can find the noise spectrum which our simulation predicted.

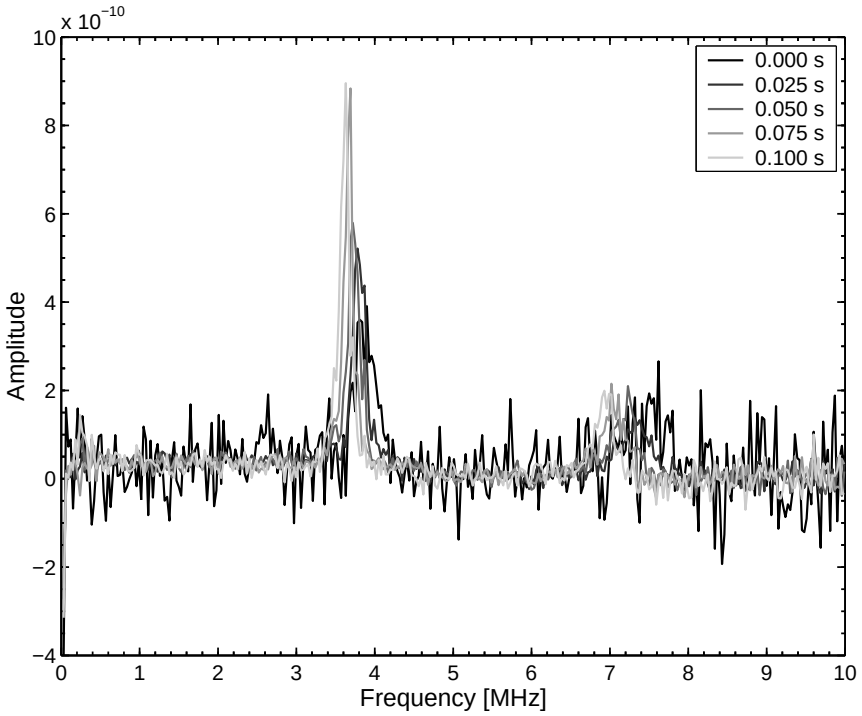

Figure 17: Ring 5, 10 MHz, current mode

6 RESULTS

6.1 The Charge Mode Success and Limitations

For the charge spectrum, our simulation predicted an exponential-like curve that becomes wider as temperature increases. Our typical spectrum consist of both mode frequencies with a Lorentizian lineshape mode frequencies and our noise spectrum. These mode frequencies are greater in amplitude than our noise spectrum. In consequence, to better observe our noise charge spectrum, we initially set our sensitivity to just see the noise spectrum and just let the mode frequencies saturate. To do this, we adjusted our sensitivity by $1/f$ where f is the frequency which it followed to get the best sensitivity possible for each frequency.

Saturated Modes Run

Fig. 18 shows the spectrum that resulted. It definitely has the same exponential-like shape as our charge spectrum in our simulation predicated. It also has an overall width that changes with time as we would expect for an electron plasma cooling in time.

After postprocessing this spectrum we concluded that we did definitely had a plasma noise temperature diagnostic which we could compare with the standard evaporation method. This postprocessing basically entails fitting our noise spectrum from our simulation to our data spectrum. For more specific details of this process, I refer back to the previous subsection in the experimental technique.

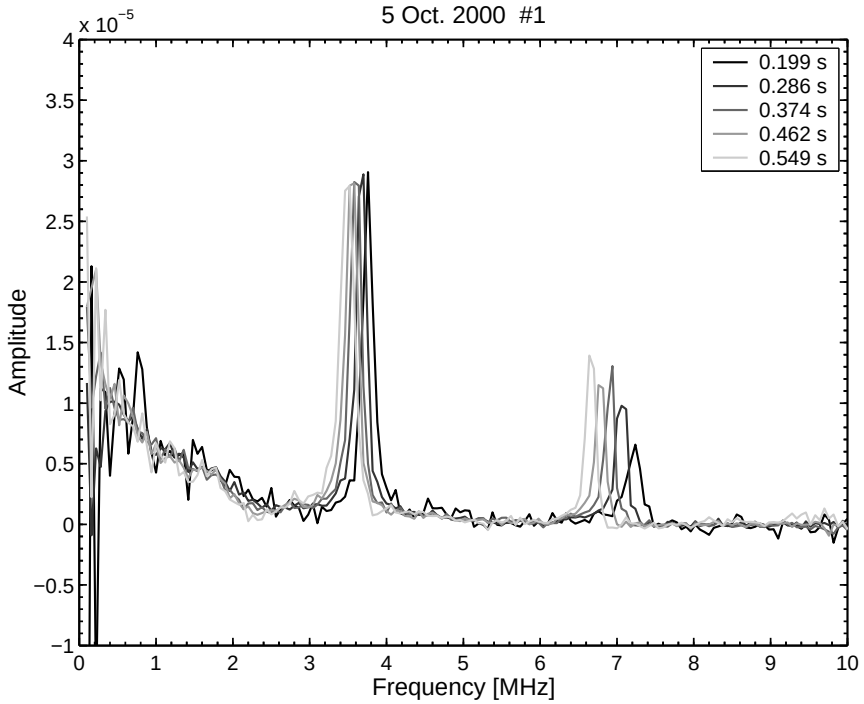

Figure 18: Saturated Modes - Amplitude vs. Frequency

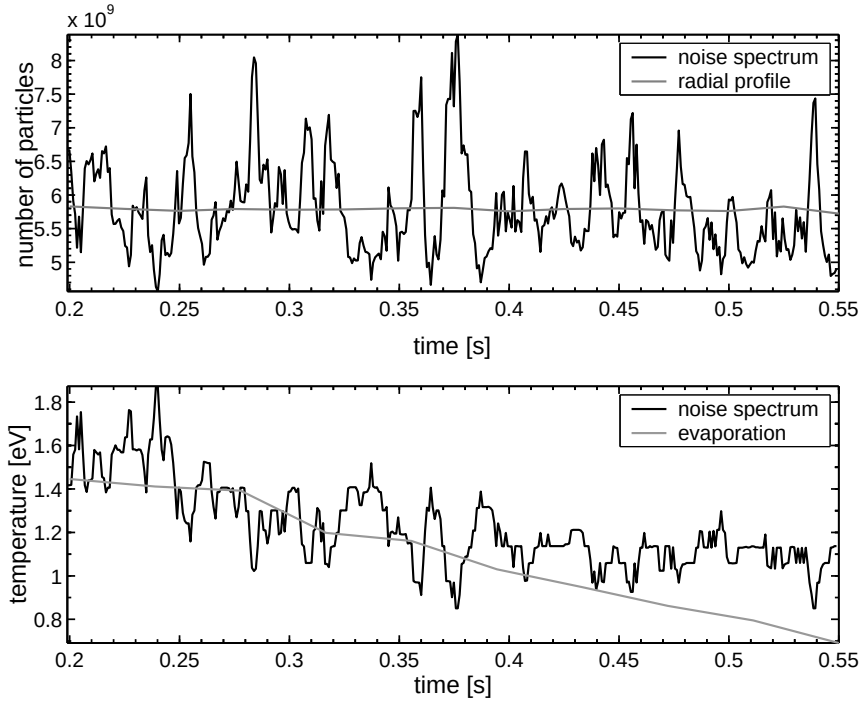

Figure 19: Saturated Modes - Temperature vs. Time

In Fig. 19 we plot both of the fitting parameters as a function of time. These parameters are the number of particles and temperature from the simulation which are used to fit to our data. Then we compare these parameters to the number of particles obtain from integrating the radial profiles and the temperature from the evaporation method.

Analysis on the Saturated Run

This plot shows that the noise spectrum method does generally follow the evaporation method until later times past 0.40 s. After 0.40 s, the evaporation method deviates from the noise spectrum method. This may demonstrate how the evaporation method is sensitive the central temperature of the plasma and the noise spectrum is sensitive to the radially averaged temperature of the plasma.

Fig. 20 shows our analysis on our simulation to better understand what parallel temperature our noise spectrum method measures. From this figure, we can see that the radially averaged temperature spectrum (0.97 eV) is the same as the radial gradient spectrum. The other 2 spectra, 0.70 eV and 1.10 eV spectra are just the extreme values for our gradient spectrum. Thus, we concluded that our noise spectrum method was sensitive to the radially averaged temperature of the plasma.

Another thing to note after 0.40 s is the fact that the plasma has expanded to the point where we would expect that the central region to be cooler than the outer region. Thus, we would expect that the temperature from the evaporation

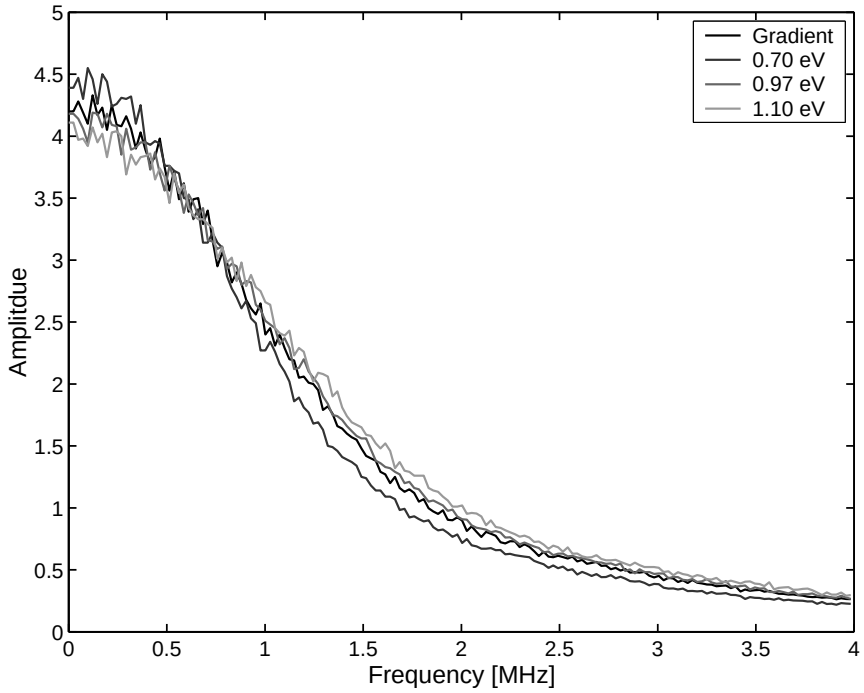

Figure 20: Spectrum with Temperature Gradient

method, which is sensitive to the center region, would be colder than that of the noise spectrum, which is sensitive to the radially averaged temperature of the plasma.

Fig. 21 shows why the outer region of the plasma is warmer than the central region of the plasma. The overall cooling mechanism for a electron plasma is collisions with neutrals. As the electrons in the central region with higher potential collide with a neutral they are knocked out to the outer region. As they are knocked down in potential, they are accelerated by the electric field which is the gradient (derivative) of this potential curve of the plasma. This results in the electrons in the outer region having more kinetic energy than their central region counterparts. In consequence, the outer region cools down more slowly than the central region.[15]

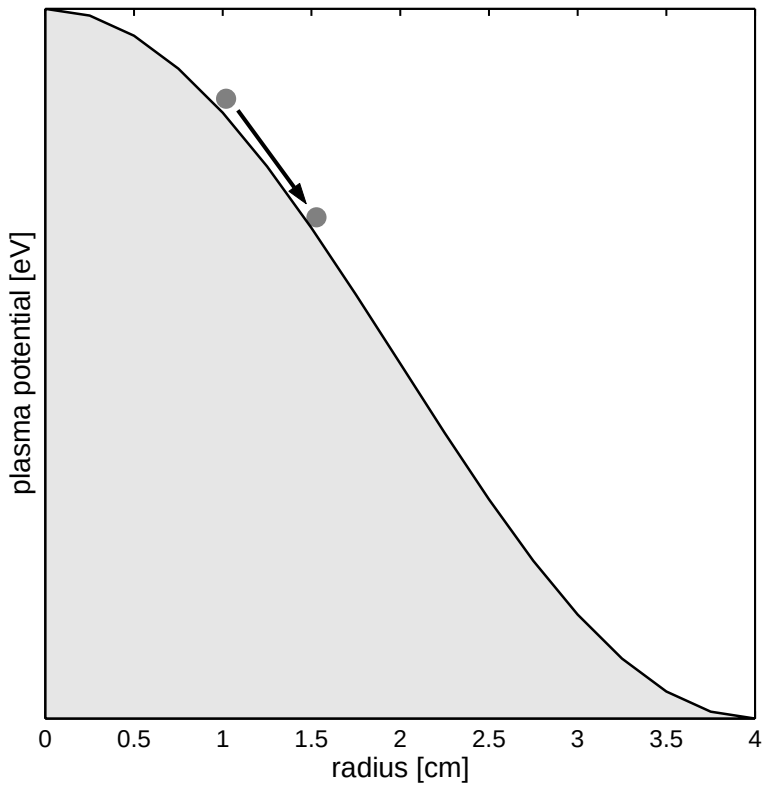

Figure 21: Why the Outer Region is Warmer?

However, the difference between the evaporation method and the noise spectrum method after 0.40 s can also possibly be accounted as hitting the noise floor when we can not tell the difference between the signal of interest and other instrumental noise.

Fig. 19 also illustrates how the fluctuations of both of these parameters are anti-correlated with each other. As the number of particles parameter from the noise spectrum is farther away in the positive direction from the normalized number of particles N like around 0.28 s, the temperature parameter from the noise spectrum is farther away in the negative direction from the evaporation method. This is

consistent with what is expected in trying to fit the spectrum from our simulation to our data spectrum. Within some limits we can make somewhat similar spectra by increasing the amplitude or decreasing the temperature.

Non-Saturated Modes Run

Fig. 22 is the experimental run where we took the full spectrum without saturating the mode frequencies. We did this by changing the sensitivity of the spectrum analyzer at each frequency so that we did not saturate near the mode frequencies.

Fig. 23 illustrates still that the noise spectrum method collected this way is comparable to the evaporation method. Both of these experimental runs, with and without saturating the mode frequencies, illustrate how the noise spectrum method generally follows the evaporation method. However, it is not as accurate as the evaporation method in that there is significant noise on the temperature fit.

In Fig. 22, we can also observe how the mode frequency shifts down in frequency and its Lorentizian lineshape grows taller and narrower as the plasma temperature decreases. Both of these characteristics can also be used to determine the parallel temperature of the plasma which will be further discussed later in this subsection.

Another Non-Saturated Run

Fig. 24 illustrates another run where the mode frequencies were not saturated. This spectrum illustrates that the plasma temperature for this run is higher than the previous run. One characteristic that hints this is the how the highest amplitude

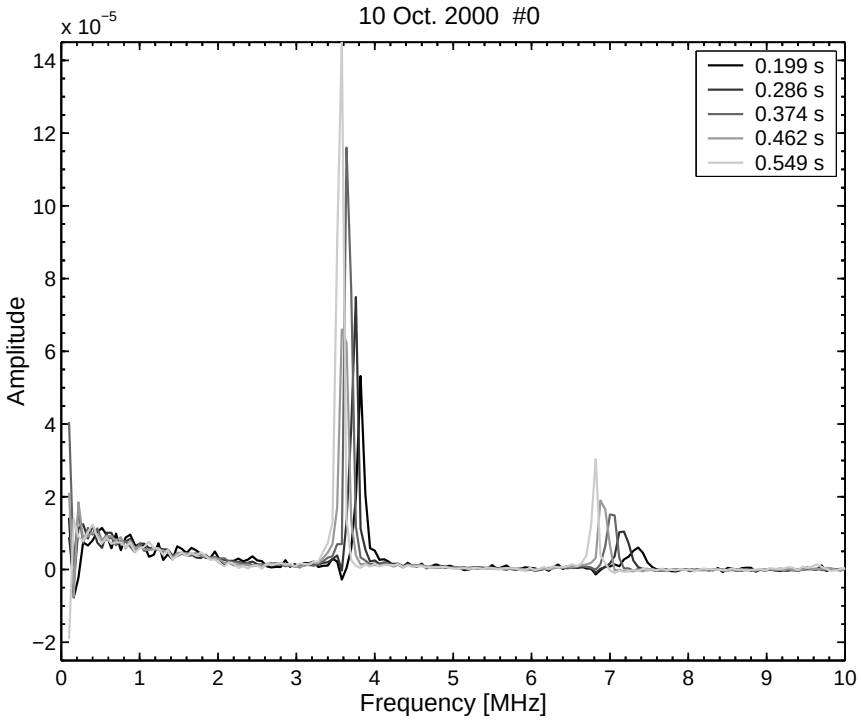

Figure 22: Non-Saturated Modes - Amplitude vs. Frequency

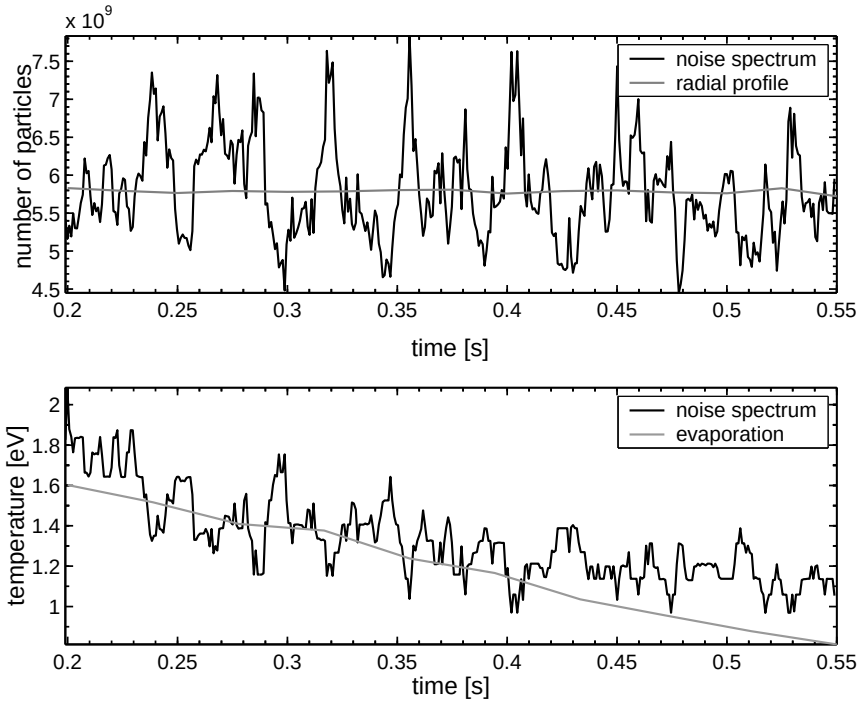

Figure 23: Non-Saturate Modes - Temperature vs. Time

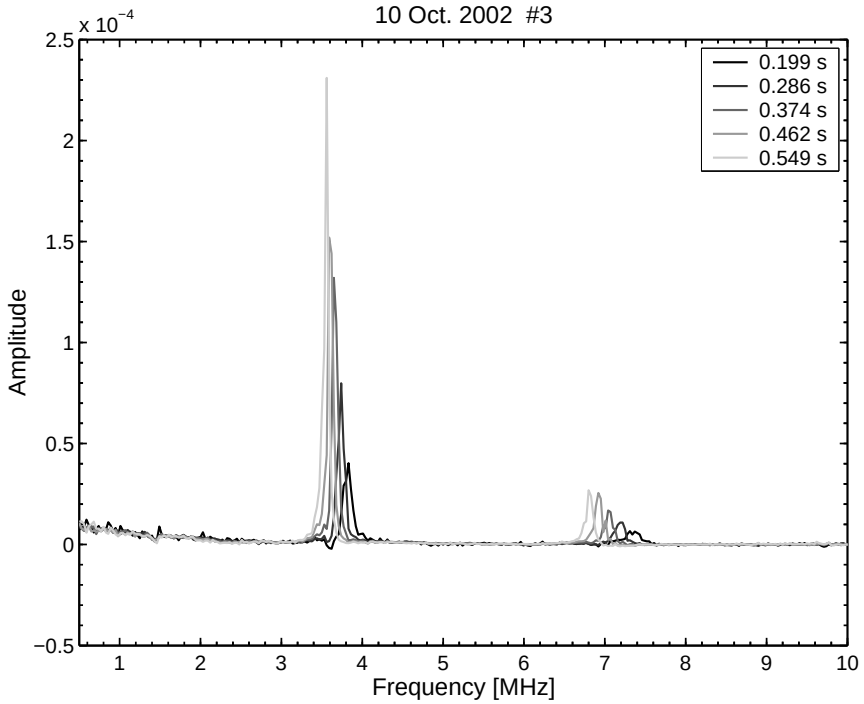

Figure 24: Second Non-Saturated Run: Amplitude vs. Frequency

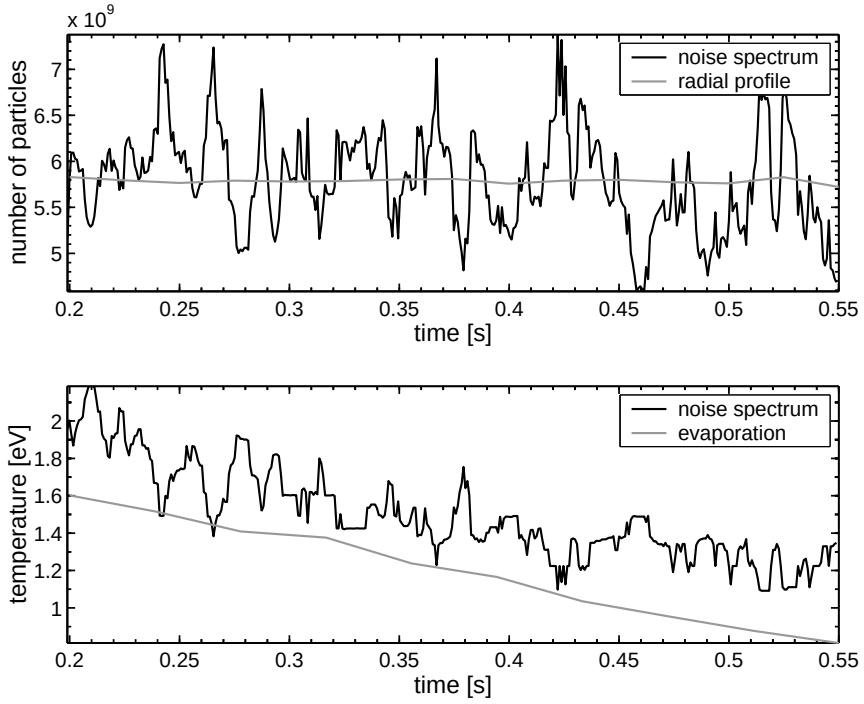

Figure 25: Second Non-Saturated Run: Temperature vs. Time

for the mode frequencies in this run is about 2.4×10^{-4} while the previous run was about 1.4×10^{-4}.

Fig. 25 illustrates that the parallel temperature is definitely at least 0.2 eV higher than in our previous run. The evaporation temperature was taken after the initial non-saturated-modes run, so it is better representative of that run.

In all of these plots it is difficult to tell anything from the number of particles part of the analysis. There seems to be a similar trend when compared to the number of particles obtained from radial profiles, but it is very noisy and not very accurate.

6.2 Other Methods

As we have noted in Fig. 22, both the mode frequency and its lorentizian shape can be used as a temperature diagnostic. Here, I would like to explain in principle how they can be used. For more details on these other methods I reference them to their respective principal investigators of these methods.

Mode Frequencies

This method to obtain the temperature using mode frequencies in the plasma was first investigated by Hansen at BYU.[2] In his investigation of this method, he excited these modes so he could get enough resolution to see them on a FFT of the time signal on an oscilliscope. Then he would take a radial profile by dumping the plasma onto the concentric collect rings. He would than use this data as input

to a computer program to calculate the temperature from the mode frequencies.

However, with the use of a spectrum analyzer, we are able to directly read of these mode frequencies in a single sweep such that we do not need to excite them. This method has been further studied by Hart.[16] However, this is a destructive method in that it requires the plasma to be dumped to get a radial profile of our plasma.

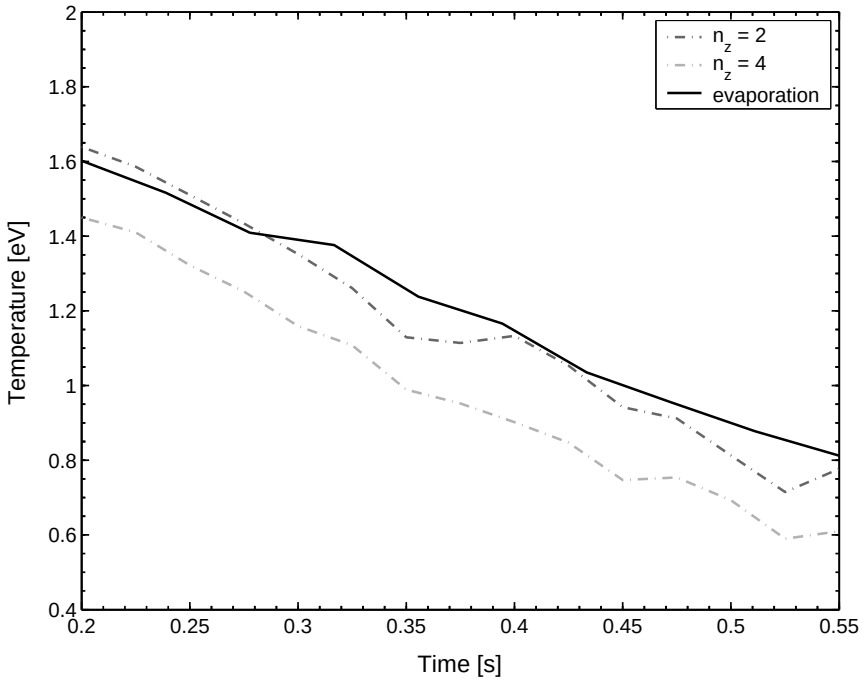

Figure 26: Mode Frequency Temperature Diagnostic

Fig. 26 illustrates the mode frequency method. As you can see both TG modes follow the evaporation method quite well through out the whole run. This makes us suspect that maybe our previous analysis on the difference between evaporation method to the noise spectrum method at later times may be that we are getting to the noise floor of our spectrum.

Mode Frequency Lineshape

This method uses the fact that energy in the Trivelpiece-Gould modes is proportional to kT. As the temperature decreases the damping increases. Simultaneously, the width of the lineshape decreases and its amplitude increases until the temperature is low enough that it decreases. All the spectra shown in our results illustrates this with their Lorentizian lineshapes. The only major drawback to this method is that it requires the impedence of the plasma which is difficult to measure.

This like the noise spectrum method, is a non-destructive temperature measurement. The only limitation is that we do need shot-to-shot reproducibility. This method is being studied by Anderegg *et al.* at UCSD and has been found to be as a reasonable non-destructive method of measuring the parallel temperature.[17]

7 CONCLUSION

7.1 Summary

In conclusion, we found out that the plasma noise spectrum can be used as a temperature diagnostic as long as we have a good signal-to-noise ratio and have no plasma modes in the 1 to 2 MHz range. We find that this method is not as practical as we had hoped because plasma modes usually dominate the range where our sensitivity to temperature is most significant. It also takes some time to obtain this measurement. However, we did find that we can get the radially averaged temperature of a nonneutral plasma by using the plasma noise spectrum.

7.2 Recommendations

For future investigation I recommend that a combination of these methods may be a possible way to obtain the parallel temperature of a non-neutral plasma confidently.

It is also possible that a single sweep in the spectrum analyzer may be a way to use the noise spectrum method to obtain temperature as long as the temperature change is slower than the spectrum analyzers sweep time. This still needs to be investigated.

Another thing to try may be to create a simulation that simulates both the mode frequencies and the noise spectrum to be used to fit to our data better. This would increase our ability to fit the data to our simulation without removing the mode frequencies.

In conclusion, one thing learned from this study is that the spectrum analyzer has given this field of research a new tool to use to probe the temperature of our plasma. As noted here we can use the spectrum analyzer to get the parallel temperature from its mode frequencies, lineshape, and the noise spectrum. Each of these methods have its strengths and difficulties. Combined though, we definitely have a viable nondestructive method to obtain the parallel temperature of a nonneutral plasma.

References

[1] D. L. Eggleston, "Parallel energy analyzer for pure electron plasma devices", *Phys. Fluids B* **4**, 3432 (1992). 1, 2.4, 4.2

[2] K. C. Hansen, *The linear and nonlinear stages of the electrostatic modes of a warm, nonneutral plasma*, Master Thesis, Brigham Young University, 1995. 1, 2, 6.2

[3] J. S. deGrassie and J. H. Malmberg, "Wave-Induced Transport in the Pure Electron Plasma", *Phys. Rev. Lett.* **39**, 1077 (1977). 2

[4] G. W. Hart, "The effect of a tilted magnetic field on the equilibrium of a pure electron plasma", *Phys. Fluids B* **3**, 2987 (1991). 2

[5] T. M. O'Neil, "A Confinement Theorem for Nonneutral Plasmas", *Phys. Fluids* **23**, 2216 (1980). 2.1

[6] K. S. Fine, *Experiments with l=1 Diocotron Mode*, PhD Thesis, University of California at San Diego, 1988. 2.2

[7] W. D. White and J. H. Malmberg, "Feedback Damping of the l=1 Dioctron Wave", *Bull. Am. Phys. Soc.* **27**, 1031 (1982). 2.2

[8] W. D. White and J. H. Malmberg, "Resistive Wall Destabilization of Diocotron Waves", *Phys. Rev. Lett.* **49**, 1822 (1982). 2.2

[9] J. H. Malmberg and J. S. deGrassie, "Properties of Nonneutral Plasma", *Phys. Rev. Lett.* **35**, 577 (1975). 2.3

[10] R. L. Spencer, "Numerical modeling of non-neutral plasmas", *AIP Conf. Proc.* **331**, 204 (1995). 2.4

[11] M. Engelson, *Modern Spectrum Analyzer Theory and Application*, Dedham, Massachusetts: Artech House, 1984. 3.1, 3.1, 4.3, 4.3, 4.3

[12] R. A. Witte, *Spectrum and Network Measurements*, Englewood Cliffs, New Jersey: Prentice Hall, 1991. 3.1, 3.1, 4.3

[13] B. G. Peterson and G. W. Hart, "Non-intrusive measurement of the longitudinal temperature of a non-neutral plasma", *Bull. Am. Phys. Soc.* **40**, 1739 (1995). 3.4

[14] B. G. Peterson and G. W. Hart, "Non-intrusive temperature measurements in a non-neutral plasma", *Bull. Am. Phys. Soc.* **41**, 1523 (1996). 3.4

[15] A. W. Hyatt, *Measurement of the Anisotropic Temperature Relaxation Rate in a Magnetized Pure Electron Plasma*, Ph.D. Diss., University of California at San Diego, 1988. 6.1

[16] G. W. Hart, B. G. Peterson, and M. T. Nakata, "Can the Plasma Mode Frequencies Be Used as a Nonneutral Plasma Temperature Diagnostic?", *Bull. Am. Phys. Soc.* **45**, 33 (2000). 6.2

[17] F. Anderegg, N. Shiga, J. R. Danielson, *et al.*, "Thermal Excitation of Trivelpiece-Gould Modes in a Pure Electron Plasma", *AIP Conf. Proc.* **606**, 253 (2002). 6.2